RESEARCH ARTICLE | MAY 31 2018

High resolution chopper spectrometer HRC and neutron Brillouin scattering FREE

Shinichi Itoh ✉; Tetsuya Yokoo; Takatsugu Masuda; Hideki Yoshizawa; Minoru Soda; Soshi Ibuka; Yoichi Ikeda; Masahiro Yoshida; Takafumi Hawai; Daichi Kawana; Ryosuke Sugiura; Toshio Asami; Yoshihisa Kawamura; Tomoko Shinozaki; Yoshiaki Ihata

AIP Conf. Proc. 1969, 050002 (2018)
https://doi.org/10.1063/1.5039299

High Resolution Chopper Spectrometer HRC and Neutron Brillouin Scattering

Shinichi Itoh[1, a)], Tetsuya Yokoo[1)], Takatsugu Masuda[2)], Hideki Yoshizawa[2)], Minoru Soda[2)], Soshi Ibuka[1)], Yoichi Ikeda[2,*)], Masahiro Yoshida[2)], Takafumi Hawai[1)], Daichi Kawana[2)], Ryosuke Sugiura[2)], Toshio Asami[2)], Yoshihisa Kawamura[2)], Tomoko Shinozaki[2)], Yoshiaki Ihata[3)]

[1]*Neutron Science Division, Institute of Materials Structure Science, High Energy Accelerator Research Organization, Tsukuba 305-0801, Japan.*
[2]*Neutron Science Laboratory, The Institute for Solid State Physics, The University of Tokyo, Tokai 319-1106, Japan.*
[3]*Materials and Life Science Experimental Facility, J-PARC Center, Tokai 319-1195, Japan.*
[*]*Present address: Institute for Material Research, Tohoku University, Sendai 980-8577, Japan.*

[a)]Corresponding author: shinichi.itoh@kek.jp

Abstract. The High Resolution Chopper Spectrometer (HRC) installed at MLF, J-PARC provides opportunities for dynamical studies of materials over a wide energy-momentum space with high resolution. Three types of inelastic neutron scattering experiments can be performed with the HRC: high-resolution experiments in a conventional energy-momentum space, eV neutron spectroscopy, and neutron Brillouin scattering (NBS). Some results have been obtained using these techniques. The NBS option makes the HRC different from other chopper spectrometers. Coherent excitations in non-single-crystal samples can be observed with NBS. On the HRC, NBS experiments were made feasible by reducing the background noise at low scattering angles, and some results were obtained.

INSTRUMENTAL DESCRIPTION

The High Resolution Chopper Spectrometer (HRC) is being operated at the 12th neutron beam line (BL12) of the Materials and Life Science Experimental Facility (MLF), Japan Proton Accelerator Research Complex (J-PARC) to study dynamics in condensed matter with high resolutions using relatively high energy neutrons [1-4]. On the HRC, a range of incident neutron energies E_i = 5 - 2000 meV is available and an energy resolution of $\Delta E/E_i$ = 2% can be achieved by using $E_i \leq 300$ meV in the best case, where the energy resolution ΔE is defined as the energy width of the elastic scattering. The layout of HRC is illustrated in Fig. 1. The HRC is a chopper spectrometer: a polychromatic pulsed neutron beam is monochromatized by a Fermi chopper and the neutrons scattered by the experimental sample are detected with a detector array covering wide scattering angles. The scattering angle (ϕ) and the time-of-flight of the detected neutron are analyzed, and then the detected neutron counts are converted to the dynamical structure factor as a function of the momentum transfer Q and the energy transfer E.

The HRC faces a decoupled moderator and sharp neutron pulses are utilized. In the primary flight path, a T0 chopper running up to 100 Hz is mounted at the 9 m position from the source and a 9.9 m long supermirror guide tube is mounted before and after the T0 chopper. A monochromatic neutron beam is produced by a Fermi chopper located at the 14 m position, and it is delivered to the sample located at the 15 m position. The available sample sizes are up to 50 mm × 50 mm for conventional experiments, and 30 mm × 30 mm for low-angle experiments. The HRC has a detector array of ^{3}He position sensitive detectors of 2.8 m long and 3/4 inch diameter located at 4 m from the sample position covering scattering angles up to ϕ = 62° for conventional experiments, and another detector array of ^{3}He position sensitive detectors of 0.8 m long and 1/2 inch diameter located at 5.2 m down to ϕ = 0.6°. Each

Proceedings of the Joint Conference on Quasielastic Neutron Scattering and the Workshop on Inelastic Neutron Spectrometers QENS/WINS 2016
AIP Conf. Proc. 1969, 050002-1–050002-5; https://doi.org/10.1063/1.5039299
Published by AIP Publishing. 978-0-7354-1676-5/$30.00

detector is mounted with its long direction being vertical. The partial pressure of ^{3}He gas is 1.8 MPa and 2 MPa for the detectors of lengths 2.8 m and 0.8 m, respectively. The background noise was successfully reduced by the T0 chopper as well as a collimator system mounted just at the upper stream of the sample. The T0 chopper is indispensable for reducing background noise originating from high energy neutrons [5]. The collimator system has two collimators composed of vertical slits of sheets of Cd, and it is effective for background noise reduction at low angles [2,4]. Either of the two collimators with 1.5° or 0.3° collimations can be selected, reducing the background noise at low angles; these collimations can reach a minimum of $\phi = 3°$ for conventional experiments and $\phi = 0.6°$ for low-angle experiments, respectively. The area of each collimator is 60 mm × 60 mm, that is larger than the beam cross section, and its length is 150 mm. A designed neutron flux at the sample position is 2×10^5 s^{-1}cm^{-2} for $E_i = 100$ meV with $\Delta E/E_i = 2.5\%$ at a beam power of 1 MW without the collimators [1]. The transmissions of the 1.5° and 0.3° collimators are 0.8 and 0.2, respectively. Namely, the neutron flux at the sample position with the 0.3° collimator is reduced to 1/4 of that with the 1.5° collimator.

The HRC can be used to perform three types of inelastic neutron scattering experiments: high-resolution experiments in a conventional energy-momentum space, eV neutron spectroscopy, and neutron Brillouin scattering (NBS). The experimental conditions for these experiments are $E_i = 5 – 500$ meV, $\phi = 3 – 62°$, $\Delta E/E_i \geq 2.5\%$, $E_i = 500 – 2000$ meV, $\phi = 0.6 – 62°$, $\Delta E/E_i \geq 5\%$, and $E_i = 100 – 300$ meV, $\phi = 0.6 – 5.1°$, $\Delta E/E_i \geq 2\%$, respectively. The dynamical structure factor can be determined in the full energy-momentum space with conventional experiments and eV neutron spectroscopy, and ferromagnetic spin waves and acoustic phonons can be observed by using polycrystalline or liquid samples with NBS.

A computational environment for controlling the experiments was developed to combine the measurements of neutron counts with the control of devices such as choppers, temperature controllers and goniometers [2]. Experiments can be performed by executing a sequence relating begin/end of measurements to the control of the devices. We also developed an original analysis program to obtain and visualize the dynamical structure factor from the accumulated neutron counts of single-crystal sample data as well as powder sample data [6,7]. The excitation spectra in the three-dimensional system on the four-dimensional energy-momentum space can be measured by rotating the sample crystal, and can hence be visualized. The analyzed data can be transformed to the standard DAVE/MSlice format [8] for convenience of users. The process for the alignment of the single crystal sample can be performed very easily.

In order to cool down the sample stably, we have a variety of sample environments: a GM-type refrigerator, a ^{3}He sorption pumping type refrigerator, and a ^{3}He circulation type refrigerator. Each refrigerator is mounted on its own goniometer. The GM-type refrigerator is conventionally used to cool the sample down to 4 K. This refrigerator exhibits a good cooling performance by improving the radiation shielding with thin Al foils. Sample temperatures as low as 2.7 K have been achieved. The lowest temperatures of 0.3 K and 0.6 K were confirmed for the ^{3}He sorption pumping type refrigerator and the ^{3}He circulation type refrigerator, respectively. For these refrigerators using ^{3}He gas, an outer vacuum chamber (OVC) is attached to separate the vacuum surrounding the sample from the vacuum scattering chamber and to maintain the lowest temperature. Background noise from the OVC and the radiation shielding for these refrigerators can be greatly reduced by operating an oscillating radial collimator [7].

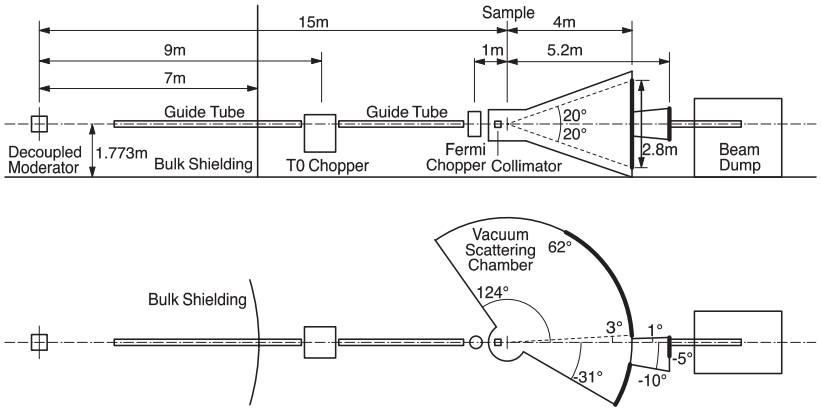

FIGURE 1. Layout of HRC. Thick lines indicate the detector arrays of ^{3}He position sensitive detectors. In the side view (upper figure), the values of the lengths are indicated. In the top view (lower figure), the values of the scattering angles (ϕ) are indicated.

IMPROVEMENT FOR NEUTRON BRILLOUIN SCATTERING

The principle of NBS is not new [9-11], and the energy-momentum space accessible by NBS has been extended by utilizing higher energy neutrons in spectrometers such as the BRISP spectrometer at ILL [12]. NBS is effective for observing coherent excitations in non-single-crystal samples such as ferromagnetic spin waves in powder samples and acoustic phonons in liquids and polycrystalline samples. In order to detect such excitations, access to the energy-momentum space near to the (000) wave-vector is required. In fact, the scattering intensity from ferromagnetic spin waves remains near to (000) only and is rapidly decayed with increasing Q by the powder average. We can access the energy-momentum space near to (000) by using low-angle detectors, high-energy neutrons and high resolution. These conditions are realized for the HRC, since it has detectors at low angles down to $\phi = 0.6°$. In Fig. 2(a), the scan locus for a detector at $\phi = 0.6°$ with $E_i = 100$ meV and the upper limit of the accessible energy-momentum space for $\phi = 5°$ are indicated. The area above this upper limit cannot be accessed using conventional spectrometers. The area between these two lines is the energy-momentum space expanded by using the NBS option of the HRC, and, at J-PARC, NBS experiments can be performed only on the HRC [3,4]. In order to realize NBS, the background noise at low angles down to $\phi = 0.6°$ was successfully reduced by the 0.3° collimator as well as by the T0 chopper, as mentioned above. The layout of the low angle detectors is also important. We can mount a detector at $\phi = 0.5°$. To use the 0.5° detector, a collimation finer than 0.3° is required with a large intensity loss. When using the 0.3° collimator, the direct beam hits the 0.5° detector. Therefore we removed the 0.5° detector, and decided to set the minimum scattering angle at $\phi = 0.6°$.

RESULTS FROM CONVENTIONAL EXPERIMENTS AND eV SPECTROSCOPY

In high-resolution experiments in the conventional energy-momentum space, several studies on condensed matter physics have been performed [13]. Some of their results are briefly summarized here. In the multiferroic system $NdFe_3(BO_3)_4$, we observed anti-crossing between spin waves of Fe ions and crystal field excitations of Nd ions, and the origin of the anisotropy was discussed [14]. In the layered nickelate $R_{2-x}Sr_xNiO_4$ (R = La and Nd), the under-doped system ($x < 0.5$) showing stripe order exhibited spin wave excitations, but the over-doped system ($x > 0.5$) with checkerboard order showed metal-like excitations [15]. In the carrier-doped Haldane system $Nd_{2-x}Ca_xBaNiO_5$ ($x = 0.1$), magnetic excitations were successfully observed in the entire Brillouin zone [16]. In eV neutron spectroscopy, some studies are in progress. The energy dependence of the absorption cross section of natural Sm shows a minimum at 0.5 eV. By using $E_i = 0.5$ eV, we successfully observed magnetic excitations in intermultiplet transitions in a skutterudite compound $SmFe_4P_{12}$ with natural Sm [17]. We have started to observe high-energy magnetic excitations in metallic antiferromagnets such as Cr [13], and we are also planning to observe electronic excitations [13].

RESULTS FROM NEUTRON BRILLOUIN SCATTERING EXPERIMENTS

We demonstrated the observation of spin waves in a polycrystalline sample of a well-known cubic perovskite ferromagnet, $La_{0.8}Sr_{0.2}MnO_3$ [3]. The observed spin wave dispersion relations (Fig. 2(a)) agreed well with the single crystal results. For a similar cubic perovskite ferromagnet $SrRuO_3$, we found a spin wave gap, as shown in Fig. 2(a) [3]. In addition, we observed spin waves from a polycrystalline sample of a strong permanent magnet $Nd_2Fe_{14}{}^{11}B$ [18], and phononic excitations in liquid D_2O [19]. The observed dispersion relations of these materials agreed well with the earlier works performed at reactor sources. The feasibility of performing NBS experiments with the HRC was demonstrated by these experiments [3,4,18,19]. Following this initial success of NBS with the HRC, many studies have been performed [20-22]. Among them, an NBS study on spin waves in the metallic ferromagnet $SrRuO_3$ [22] is briefly described here.

$SrRuO_3$ is a rare material showing a ferromagnetic transition among 4d electron systems: it orders ferromagnetically at $T_C = 165$ K, takes a nearly-cubic perovskite type crystal structure, and shows good electric conductivity at low temperatures. Typically, cubic ferromagnets such as Fe, Ni, and $La_{0.8}Sr_{0.2}MnO_3$ show very little magnetic anisotropy, and therefore, the spin wave gap is negligibly small. On the other hand, $SrRuO_3$ shows a large magnetic anisotropy and a finite spin wave gap is observed, as shown in Fig. 2(a). Further, $SrRuO_3$ shows an anomalous Hall resistivity that is not proportional to the magnetization [23]. In $SrRuO_3$, the band structure shows a

band crossing due to the spin-orbit interaction, which produces the Berry phase. The Berry curvature of the band crossing takes the form of the magnetic field of a monopole in the momentum space, and the fictitious magnetic field of the monopole is an origin of the anomalous Hall effect: the anomalous Hall conductivity σ_{xy} is described by the Berry curvature. The anomalous Hall effect in $SrRuO_3$ is well explained by this model [23]. We attempted to detect this fictitious magnetic field by inelastic neutron scattering.

However, for $SrRuO_3$, a sufficiently large single crystal, as is necessary for inelastic neutron scattering, has not been synthesized until very recently. In view of this, we performed the NBS experiment with the HRC by using a polycrystalline sample, and well-defined spin-wave peaks were observed at temperatures (T) below T_C. The obtained spin-wave dispersion curve at any T can be well fitted to $E(Q) = DQ^2 + E_g$, and the stiffness constant D and spin-wave gap E_g were determined as a function of T. The spin-wave gap E_g shows non-monotonic T dependence, as shown in Fig. 2(b). We found that the observed spin-wave gap can be well explained by the theoretical function, $E_g(T) = aM(T)/[1+bM(T)\sigma_{xy}(T)]$ with adjustable parameters a and b. In this analysis, experimental data for the magnetization $M(T)$ and the anomalous Hall conductivity $\sigma_{xy}(T)$ were used: $M(T)$ shows monotonic T dependence, whereas $\sigma_{xy}(T)$ shows non-monotonic T dependence, as shown in the inset of Fig. 2(b). For the band crossing, the Weyl fermion described by the Hamiltonian $H = v(\mathbf{k}-\mathbf{k}_0)\boldsymbol{\sigma}$ is considered, where $\mathbf{k}$ is the momentum, $\mathbf{k}_0$ is the Weyl point (band crossing point), $\boldsymbol{\sigma}$ is Pauli's spin matrices, and v is a constant; the generalized susceptibility can be described as a function of σ_{xy} described by the Berry curvature. Therefore, inelastic neutron scattering detects the Berry phase or the fictitious magnetic field of monopoles through the anomalous Hall conductivity σ_{xy}. Until this study, Weyl fermions were discussed only in transport phenomena, in terms of spintronics. We showed experimentally that the Berry curvature is an observable of inelastic neutron scattering and that the spin dynamics directly reflects Weyl fermions [22]. This result has revealed the novel connection between the transport and dynamical magnetic properties through the enhanced spin-orbit coupling effect.

SUMMARY

With the HRC, in high-resolution experiments in the conventional space and eV neutron spectroscopy, several studies have been performed and others are currently in progress. We realized NBS experiments with the HRC by using high-energy neutrons at low angles and high resolution, with a successful reduction of background noise at low angles. The NBS option makes the HRC different from other chopper spectrometers, and opens opportunities for contributing current science by measuring coherent excitations from non-single-crystal samples.

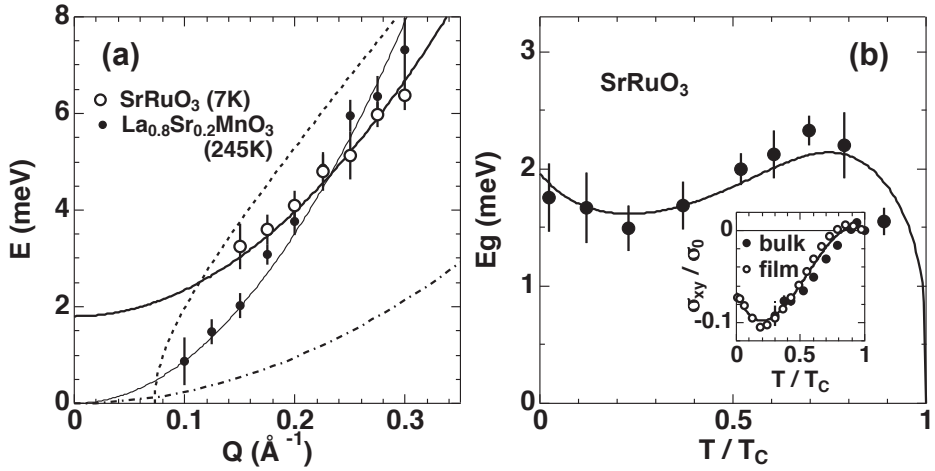

FIGURE 2. (a) Dispersion relations of spin waves in $SrRuO_3$ (T = 7 K) and $La_{0.8}Sr_{0.2}MnO_3$ (T = 245 K) observed with the HRC with fitted curves $E(Q) = DQ^2 + E_g$ [3]. The dashed line is the scan locus for a detector at $\phi = 0.6°$ and with E_i = 100 meV, and the chain line is the upper limit of the accessible energy-momentum space for $\phi \geq 5°$. (b) T dependence of the spin-wave gap E_g for $SrRuO_3$ [22]. The solid line is a curve fitted with the theoretical function described in the text. The inset shows the T dependence of the anomalous Hall conductivity σ_{xy} for bulk and film samples, where T_C = 165 K and σ_0 is a constant, and the solid line is an empirical function describing $\sigma_{xy}(T)$ for the analysis of $E_g(T)$.

ACKNOWLEDGMENTS

The neutron scattering experiments were approved by the Neutron Scattering Program Advisory Committee of the Institute of Materials Structure Science, High Energy Accelerator Research Organization (Nos. 2012S01, 2013S01, 2014S01, 2015S01 and 2016S01). We thank S. Hayashida, S. Suzuki, T. Nakabayashi, K. Kuwahara, H. Hiraka, K. Yoshida, K. Ono, M. Fujita, Y. Kaneko, K. S. Takahashi, Y. Tokura, N. Nagaosa and Y. Endoh for the collaborations.

REFERENCES

1. S. Itoh, T. Yokoo, S. Satoh, S. Yano, D. Kawana, J. Suzuki,T. J. Sato, Nucl. Instr. Meth. Phys. Res. A **631**, 90 – 97 (2011).
2. S. Itoh, T. Yokoo, D. Kawana, H. Yoshizawa, T. Masuda, M. Soda, T. J. Sato, S. Satoh, M. Sakaguchi, S. Muto, J. Phys. Soc. Jpn. **82**, SA033 (2013).
3. S. Itoh, Y. Endoh, T. Yokoo, D. Kawana, Y. Kaneko, Y. Tokura and M. Fujita, J. Phys. Soc. Jpn. **82**, 043001 (2013).
4. S. Itoh, T. Yokoo, D. Kawana and Y. Endoh, J. Phys. Soc. Jpn. **82**, SA034 (2013).
5. S. Itoh, K. Ueno, R. Ohkubo, H. Sagehashi, Y. Funahashi and T. Yokoo, Nucl. Instr. Meth. Phys. Res. A **661**, 86 – 92 (2012).
6. D. Kawana, M. Soda, M. Yoshida, Y. Ikeda, T. Asami, R. Sugiura, H. Yoshizawa, T. Masuda, T. Hawai, S. Ibuka, T. Yokoo, S. Itoh, to be presented at the 22nd meeting of the International Collaboration on Advanced Neutron Sources (ICANS XXII), 27 - 31 March 2017, Oxford, UK.
7. S. Itoh, T. Yokoo, T. Masuda, H. Yoshizawa, M. Soda, Y. Ikeda, S. Ibuka, M. Yoshida, T. Hawai, T. Asami, R. Sugiura, D. Kawana, Y. Kawamura, T. Shinozaki, Y. Ihata, J-PARC Annual Report 2015, vol. 2, pp.86 - 87 (J-PARC 17-01, J-PARC Center, 2017).
8. R.T. Azuah, L.R. Kneller, Y. Qiu, P.L.W. Tregenna-Piggott, C.M. Brown, J.R.D. Copley, R.M. Dimeo, J. Res. Natl. Inst. Stan. Technol. **114**, 341 – 358 (2009).
9. L. Passell, O.W. Dietrich, J. Als-Nielsen, Phys. Rev. B **14**, 4897 – 4907 (1976).
10. Y. Ishikawa, K. Yamada, K. Taijma, K. Fukamachi, J. Phys. Soc. Jpn. **50**, 1958 – 1963 (1981).
11. R.A. Robinson, Physica B **156 & 157**, 557 – 560 (1989).
12. D. Aisa, S. Aisa, E. Babucci, F. Barocchi, A. Cunsolo, A. De Francesco, F. Formisano, T. Gahl, E. Guarini, A. Laloni, H. Mutka, A. Orecchini, C. Petrillo, W.-C. Pilgrim, A. Piluso, F. Sacchetti, J.-B. Suck, G. Venturi, J. Non-Crystalline Solids **352**, 5130 – 5135 (2006).
13. S. Itoh, T. Yokoo, T. Masuda, H. Yoshizawa, M. Soda, Y. Ikeda, D. Kawana, T. J. Sato, Y. Nambu, K. Kuwahara, S. Yano, J. Akimitsu, Y. Kaneko, Y. Tokura, M. Fujita, M. Hase, K. Iwasa, H. Hiraka, T. Fukuda, K. Ikeuchi, K. Yoshida, T. Yamaguchi, K. Ono, Y. Endoh, JPS Conf. Proc. **8**, 034001 (2015).
14. S. Hayashida, M. Soda, S. Itoh, T. Yokoo, K. Ohgushi, D. Kawana, H. M. Rønnow, T. Masuda, Phys. Rev. B **92**, 054402 (2015).
15. Y. Ikeda, S. Suzuki, T. Nakabayashi, H. Yoshizawa, T. Yokoo, S. Itoh, J. Phys. Soc. Jpn. **85**, 023701 (2016).
16. T. Yokoo, S. Itoh, D. Kawana, H. Yoshizawa, J. Akimitsu, J. Phys.: Conf. Series **502**, 012045 (2014).
17. S. Konno, A. Ssuzuki, K. Nihei, K. Kuwahara, D. Kawana, T. Yokoo, S. Itoh, J. Phys.: Conf. Series **592**, 012029 (2015).
18. K. Ono, N. Inami, K. Saito, Y. Takeichi, M. Yano, T. Shoji, A. Manabe, A. Kato, Y. Kaneko, D. Kawana, T. Yokoo, S. Itoh, J. Appl. Phys. **115**, 17A714 (2014).
19. S. Itoh, T. Yokoo, D. Kawana, Y. Kaneko, Y. Tokura, M. Fujita, K. Yoshida, K. Saito, N. Inami, Y. Takeichi, K. Ono, Y. Endoh, J. Phys.: Conf. Series **502**, 012043 (2014).
20. K. Yoshida, T. Yamaguchi, T. Yokoo, S. Itoh, J. Molecular Liquids **222**, 395 – 397 (2016).
21. S. Hosokawa, K. Kimura, M. Yamasaki, Y. Kawamura, K. Yoshida, M. Inui, S. Tsutsui, A.Q.R. Baron, Y. Kawakita, S. Itoh, J. Alloys and Compounds **695**, 426 – 432 (2017).
22. S. Itoh, Y. Endoh, T. Yokoo, S. Ibuka, J.-G. Park, Y. Kaneko, K.S. Takahashi, Y. Tokura, N. Nagaosa, Nature Communications **7**, 11788 (2016).
23. Z. Fang, N. Nagaosa, K.S. Takahashi, A. Asamitsu, R. Mathieu, T. Ogasawara, H. Yamada, M. Kawasaki, Y. Tokura, K. Terakura, Science **302**, 92 – 95 (2003).